ACS APPLIED MATERIALS & INTERFACES

Research Article

www.acsami.org

Photoelectrochemical Water Splitting Promoted with a Disordered Surface Layer Created by Electrochemical Reduction

Pengli Yan,[†,‡] Guiji Liu,[‡,§] Chunmei Ding,[‡,§] Hongxian Han,[‡] Jingying Shi,[‡] Yang Gan,*[,†] and Can Li*[,‡]

[†]School of Chemical Engineering & Technology, Harbin Institute of Technology, Harbin 150001, China

[‡]State Key Laboratory of Catalysis, Dalian Institute of Chemical Physics, Chinese Academy of Sciences and Dalian National Laboratory for Clean Energy, Dalian 116023, China

[§]University of Chinese Academy of Sciences, Beijing 100049, China

Supporting Information

ABSTRACT: The recent discovery of colored TiO_2 indicated that the disordered surface layer over the TiO_2 particles/photoelectrodes is beneficial for higher photocatalytic performance; however, the role of the disordered surface TiO_2 layer is not well understood. Here, we report an electrochemical strategy for tuning the surface structure of TiO_2 nanorod arrays (NRAs) and try to understand the role of the disordered surface TiO_2 layer. Photoelectrodes of TiO_2 NRAs with a disordered shell were prepared by an electrochemical reduction method. The photocurrent of the NRAs with a disordered shell can reach as high as ~1.18 mA/cm^2 at 1.23 V, which is 2.2 times of that of the pristine TiO_2 NRAs. Our results show that the surface disordered layer not only improves the bulk charge separation but also suppresses the charge recombination at the electrode/electrolyte interface, acting as an efficient water oxidation cocatalyst of photoelectrochemical cell for solar water splitting.

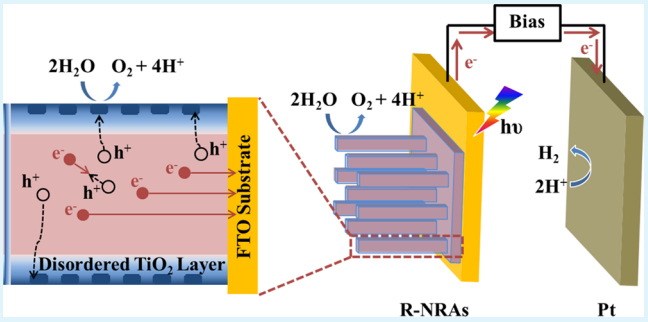

KEYWORDS: *TiO_2 nanorod arrays, surface disordered layer, electrochemical reduction, water splitting, charge injection efficiency*

1. INTRODUCTION

Photoelectrochemical (PEC) water splitting is an ideal method for hydrogen production. In a single PEC system, solar energy harvesting and water electrolysis is integrated.[1−3] Various configurations of PEC water splitting cells using semiconductor photoelectrodes have been developed in the past 40 years.[4−9] One of the key factors governing the PEC water splitting is the semiconductor/liquid interface where the surface reactions take place. Accordingly, attempts to engineer the semiconductor/electrolyte interface have drawn increasing attention recently.[10−14]

Modification of semiconductor with a surface overlayer has been used to tune the semiconductor/electrolyte interface. Improved PEC water splitting performance of hematite, for instance, has been achieved when the surface was passivated by Al, Ga and In oxide overlayers.[15] Hole conduction on narrow bandgap semiconductor photoanodes was also promoted in the presence of a surface TiO_2 amorphous layer.[16] The outmost amorphous layer on (oxy)nitrides, however, was found to be detrimental to the photocatalytic activity.[17−19] Clearly, these different experimental results indicate that formation of a surface overlayer directly affects the PEC performance.

The colored TiO_2 prepared by various reduction treatments has a unique hydrogenated disordered shell.[20−22] The disordered surface layer is beneficial to the charge-transfer process,[23] as a result, the efficient H_2 production of colored TiO_2 is, at least in part, related to the formation of disordered surface layer. However, to achieve better PEC performance, high temperature or pressure is usually required during the hydrogen treatment.[24,25] Alternately, electrochemical reduction has also been demonstrated to be a straightforward approach for higher electrochemical and PEC activity.[26,27] However, to the best of our knowledge, the role of the TiO_2 semiconductor/electrolyte interface has been rarely reported for the electrochemically reduced TiO_2.

Herein, we demonstrate that an electrochemically reduced TiO_2 overlayer can significantly influence the semiconductor/electrolyte interface property of TiO_2 photoanode which is used as a prototype for the investigation of charge separation and collection at the surface layer. Specifically, the TiO_2 rutile nanorod arrays (NRAs) photoanodes were modified with a disordered surface layer by a facile electrochemical method. Compared with the pristine NRAs, the introduction of the disordered surface layer leads to about 2.2 times of photocurrent enhancement at 1.23 V versus reversible hydrogen electrode (vs RHE), which is very likely due to the the

Received: December 11, 2014
Accepted: January 26, 2015
Published: January 26, 2015

DOI: 10.1021/am508738d
ACS Appl. Mater. Interfaces 2015, 7, 3791−3796

disordered TiO_2 layer acting as both charge separation layer and oxygen evolution catalyst.

2. EXPERIMENTAL SECTION

2.1. Growth of Rutile TiO_2 Nanorod Arrays. The TiO_2 NRAs were grown on fluorine-doped tin oxide (FTO) glass by a hydrothermal method.[28] One-tenth of a milliliter of tetrabutyl titanate (Alfa Aesar, 99%) was added dropwise into 10 mL of HCl aqueous solution (6 M). The solution was transferred into a 30 mL Teflon-lined stainless autoclave with a piece of precleaned FTO glass (ultrasonically cleaned with acetone, isopropanol, ethanol and deionized water for 20 min in sequence). The autoclave was then put into an oven and kept at 180 °C for 2 h and allowed to cooled down to room temperature naturally. Finally, the NRAs were rinsed with copious deionized water and annealed at 450 °C for 2 h in a muffle furnace.

2.2. Electrochemical Reduction of TiO_2 NRAs. The electrochemical reduction was carried out in a conventional three-electrode system connected to a potentiostat (Iviumstat, Ivium Technologies). The pristine NRAs, a saturated calomel electrode (SCE) and platinum plate were used as working, reference and counter electrodes, respectively. Na_2SO_4 aqueous solution (0.5 M, pH 6.8) was used as electrolyte; the reduced NRAs were denoted as R-NRAs. The external bias of −1.6, −1.7, −1.8, −1.9, −2.0, and −3.0 V (vs SCE) were applied and the obtained photoelectrodes are denoted as −1.6, −1.7, −1.8, −1.9, −2.0, and −3.0 V, respectively. The R-NRAs were also performed at applied bias of −1.8 V for the reduction period of 0.5, 1, 2, 5, and 10 s. Unless otherwise specified, the external biases were compared with SCE.

2.3. Electrodeposition of Oxygen Evolution Catalyst. CoPi cocatalyst was electrodeposited on NRAs and R-NRAs at 0.59 V vs SCE in 0.1 M sodium phosphate buffer solution (buffered at pH 7) containing 1 mM Co^{2+}.[7] The loading amount of CoPi was controlled by the electric charge passed per geometric area (10 mC cm^{-2} unless otherwise stated).

2.4. Sample Characterization. The morphology of rutile TiO_2 NRAs and R-NRAs were examined using a field emission scanning electron microscopy (SEM, Quanta 200 FEG, accelerating voltage of 20 kV). High resolution transmission electron microscopy (HRTEM) images were obtained on a Tecnai G2 F30 S-Twin (FEI Company) with an acceleration voltage of 300 kV. The X-ray diffraction (XRD, Rigaku Rotaflex Ru-200 B) patterns were performed with Cu−Kα radiation (operating voltage: 40 kV, operating current: 200 mA, scan rate: 5° min^{-1}). UV−vis diffuse reflectance spectra (UV−vis) were recorded on an UV−vis spectrophotometer (JASCO V-550) equipped with an integrating sphere. X-ray photoelectron spectroscopy (XPS) measurements were performed using a Thermo ESCALAB 250Xi with monochromatized Al Kα excitation. Raman scattering measurements were recorded with a 325 nm laser line as exciting light. The thickness of the film was determined with a Stylus Profilometry (Dektak XT). The EPR measurements were carried out on a Bruker EPR A200 spectrometer. The samples (about 2 × 10 mm^2) were placed into a homemade EPR quartz tube, and the tube was vacuumized and ventilated with argon before placed inside the microwave cavity. For comparison, all of the EPR spectra were recorded under the same experimental conditions with the following EPR parameter settings: temperature, 100 K; microwave frequency, 9.30 GHz; center field, 3300 G; sweep width, 600 G; modulation frequency, 100 kHz; and power, 2.00 mW.

2.5. Photoelectrochemical Measurements. The PEC tests were conducted with an electrochemical workstation (Iviumstat, Ivium Technologies) and a conventional three-electrode system. Illumination source was a 150 W Xe lamp coupled with an AM 1.5G filter (100 mW cm^{-2}, Newport Sol 3A, Class AAA Solar simulator). Otherwise mentioned, 0.5 M Na_2SO_4 aqueous solution (pH 6.8) was used as electrolyte. The photocurrent was measured by linear sweep voltammetry with a scan rate of 50 mV s^{-1}. Unless otherwise specified, the potential was referred to RHE. The incident photon to current efficiency (IPCE) was evaluated under monochromatic light irradiation, the illumination was provided by a tungsten lamp equipped with a monochromator (CROWNTECH, QEM24-D 1/4 m Double). The light intensity was calibrated with a standard Si photodiode. Mott−Schottky plots were evaluated at DC potential range of −0.4−0.2 V vs RHE at a frequency of 1 kHz in dark. Electrochemical impedance spectroscopies (EIS) were carried out at a potentials of 0.64 V vs RHE, with an AC potential frequency range from 100 K to 0.1 Hz under AM 1.5G simulated sunlight at 100 mW cm^{-2} in 0.5 M Na_2SO_4 electrolyte. The program ZView (Scribner Associates Inc.) was used to fit the obtained data to the corresponding equivalent circuit model.

3. RESULTS AND DISCUSSION

3.1. Characterization of NRAs. The NRAs were synthesized by a typical hydrothermal method,[28] followed by annealing in air at 500 °C. Figure 1a shows the SEM image of the white TiO_2 film obtained on FTO substrate. The pristine TiO_2 film consists of dense and vertically aligned nanorod arrays. The nanorods are tetragonal in shape with a square facet on the top ranging from 80 to 200 nm and a mean length of 2.0 μm. The XRD pattern of NRAs (see Figure S1 in the Supporting Information) shows two sharp peaks centered at 36.5 and 63.2°, which correspond to (101) and (002) diffraction peaks of rutile TiO_2 (JCPDS No.21−1276).

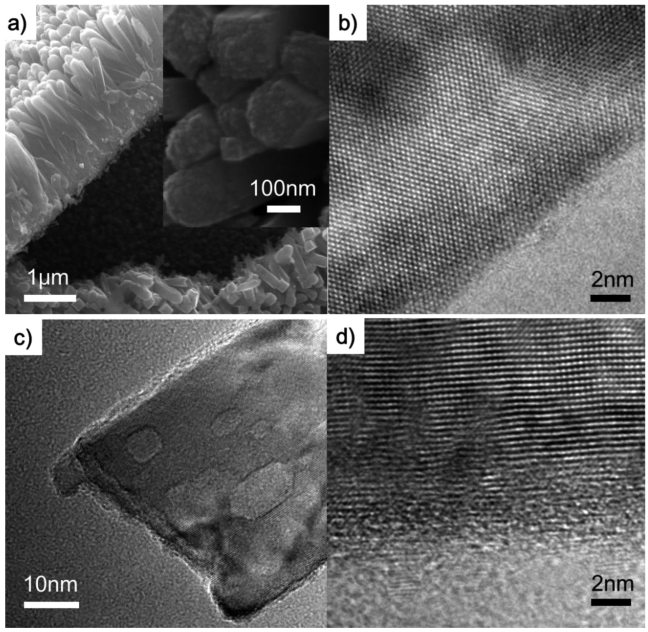

Figure 1. (a) SEM image of NRAs prepared by hydrothermal method and the inset is magnified image of the NRAs; (b) HR-TEM images of the NRAs nanorod; (c) TEM and (d) HR-TEM images of R-NRAs electrochemically reduced under the applied bias of −1.8 V vs SCE for 2 s.

3.2. Surface Modification of NRAs with an Electrochemical Reduction Method. The pristine NRAs were electrochemically reduced under different external biases. After the reduction, the morphology of R-NRAs remains as that of the pristine NRAs (see Figure S2 in the Supporting Information); however, the color of R-NRAs turns into light to dark gray varying with the applied potentials. The main UV−visible spectra of NRAs and R-NRAs show no difference on the absorption band edge (see Figure S3 in the Supporting Information). Additional weak absorption in the extended region up to 800 nm for the R-NRAs indicates that some

DOI: 10.1021/am508738d
ACS Appl. Mater. Interfaces 2015, 7, 3791−3796

shallow states energy levels form between the conduction and valence band.[29]

To examine the refined morphology changes during the electrochemical reduction, we characterized a single nanorod with HRTEM. As shown in Figure 1b, the pristine rutile nanorod shows lattice fringes with d_{110} = 3.2 Å and d_{101}= 2.5 Å. However, after the electrochemical reduction, the nanorod is capped with a ~4 nm shell (Figure 1c). The lattice fringe of the core is attributed to the rutile (110) crystal planes, whereas the shell is disordered (Figure 1d). Moreover, the disordered layer disappears once the R-NRAs are annealed in air at 450 °C for 30 min.

3.3. Photoelectrochemical Water Oxidation on R-NRAs. The *J*−*V* curves of the R-NRAs were measured in 0.5 M Na_2SO_4 aqueous solution. Figure 2a shows that the onset potentials of the R-NRAs exhibit a cathodic shift of 50−150 mV compared with that of the pristine NRAs. The steady state current profiles of the R-NRAs and pristine NRAs further confirm the cathodic shift in the onset potential (see Figure S4 in the Supporting Information). Moreover, the photocurrent densities of the R-NRAs increase steeply to a saturated value at 1.2 V, representing a higher fill factor. The R-NRAs electrode prepared under −1.8 V vs SCE yields a maximum photocurrent density of 1.18 mA/cm^2 at 1.23 V (inset in Figure 2a), which is 2.2 times of that of the pristine NRAs. The stabilities of NRAs and R-NRAs electrodes (reduced at −1.8 V) were measured for prolonged period of 5 h at 1.23 V under AM 1.5G simulated sunlight. Notably, both NRAs and R-NRAs electrodes show stable photocurrent under irradiation for 5 h (Figure 2b), suggesting that the increase in photocurrent in the LSV curve is mainly due to water oxidation instead of oxidation of some other reduced species. Obviously, the photocurrent density enhancement is related to the applied bias. When the reduction bias is more negative than −1.8 V, the photocurrent densities of R-NRAs decrease due to the reduction of the FTO substrate (see Figure S5 in the Supporting Information). It was also found that the more negative potentials lead to the increase in the shell thickness (see Figure S6 in the Supporting Information). Accordingly, it is natural to deduce that the improved activity of R-NRAs can be attributed to the appearance of the disordered surface layer.

It is expected that prolonging the reduction time under a constant bias can result in a similar photocurrent change. Figure 2c shows that the R-NRAs electrode after 2 s reduction yields a maximum photocurrent density (the inset in Figure 2c). Because of the reduction of the FTO substrate, the photocurrent density of the R-NRAs decreased when the reduction time was over 2 s. These results are in accordance with the trend obtained at Figure 2a. Moreover, the NRAs and R-NRAs electrodes are oxidized at 2.0 V vs SCE for 2 s (see Figure S7 in the Supporting Information), based on the almost unchanged *J*−*V* curves of NRAs and R-NRs before and after oxidation at 2.0 V vs SCE, it seems the rutile nanorod and the disordered surface layer is not oxidized at a high positive bias.

As shown above, the presence of a disorder surface layer has significant influence on the PEC performance of TiO_2 NRAs. To understand this phenomenon, we conducted more characterizations of the disordered layer. UV Raman spectra of NRAs and R-NRAs show no significant differences (see Figure S8 in the Supporting Information), which is consistent with conclusion of no obvious structure changes drawn by the study of the HRTEM images. The cyclic voltammetry curves for the NRAs and FTO substrates recorded during the

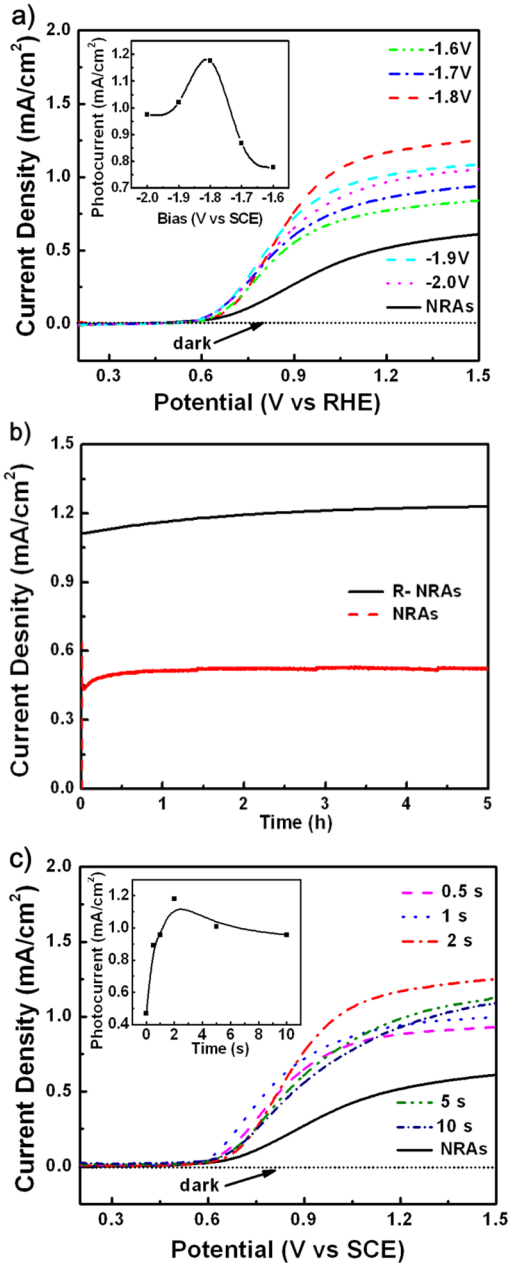

Figure 2. (a) Current density versus potential curves for the NRAs and R-NRAs prepared under different applied bias for 2 s, the inset is the photocurrent density for R-NRAs at 1.23 V vs RHE as a function of the external bias for electrochemical reduction. (b) Chronoamperometry measurements of the NRAs and R-NRAs (reduced under −1.8 V for 2 s) photoanodes at 1.23 V. (c) Current density versus potential curves for the NRAs and R-NRAs prepared under −1.8 V for several seconds; the inset is the photocurrent density for R-NRAs at 1.23 V as a function of reduction time.

reduction process (see Figure S9 in the Supporting Information) imply that hydrogen evolution occurs at the interface between the NRAs and the electrolyte. The X-ray photoelectron spectroscopy (XPS) spectra shown in Figure 3a indicates that the Ti 2p spectra of the NRAs can be deconvoluted by the Ti 2p3/2 and the Ti 2p1/2 peaks centered at a binding energy of 464.6 and 458.8 eV, respectively. These two peaks are due to the presence of Ti^{4+}.[25] On the contrary, These two peaks of R-NRAs were negatively shifted to 463.9 and 458.0 eV, suggesting the

DOI: 10.1021/am508738d
ACS Appl. Mater. Interfaces 2015, 7, 3791−3796

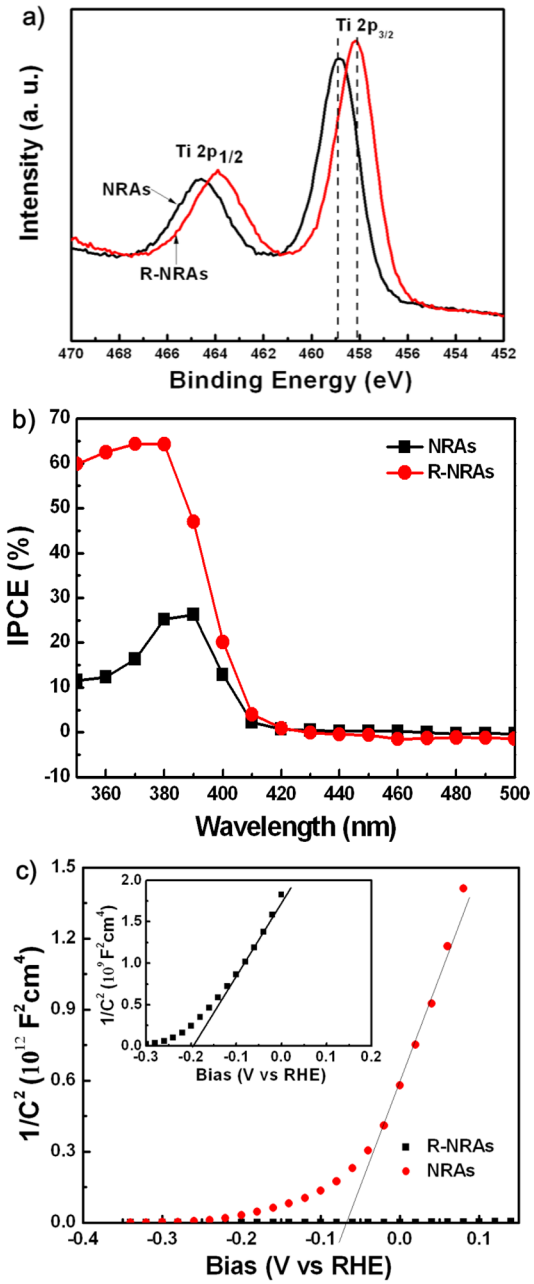

Figure 3. (a) Ti 2p spectra of the NRAs and R-NRAs; (b) IPCE spectra of the NRAs and R-NRAs reduced under −1.8 V, collected at a potential of 1.23 V vs RHE; (c) Mott−Schottky plots collected at a frequency of 1 kHz in the dark for the NRAs and R-NRAs. Inset: Mott−Schottky plots of the R-NRAs reduced under −1.8 V, collected under the same conditions.

presence of Ti^{3+} ($Ti^{4+} + e^- \rightarrow Ti^{3+}$).[26] EPR spectra (100 K) of the NRAs and R-NRAs (see Figure S10 in the Supporting Information) also show that both signals of trapped holes ($Ti^{4+}O^{2-}Ti^{4+}OH^- + h^+ \rightarrow Ti^{4+}O^{\bullet}Ti^{4+}OH^-$, g = 2.003) and trapped electrons ($Ti^{4+} + e^- \rightarrow Ti^{3+}$, $g_\perp$ = 1.973, $g_\parallel$ = 1.944) increase after the reduction;[30,31] moreover, the $O^{\bullet-}$ signal enhances as the bias decreases. The O 1s spectra of the NRAs and R-NRAs (see Figure S11 in the Supporting Information) both consist of two peaks centered at 529.5 and 531.4 eV. The peak of Ti−OH at 531.4 eV increases after electro-reduction,[26] which confirms the formation of hydroxyl groups on TiO_2 surface during reduction. The above results suggest that oxygen vacancies might be introduced into the disordered shell.

The shallow states energy levels in the disordered surface layer might result in extended light absorption. However, the incident-photon-to-current-conversion efficiency (IPCE) measurement (Figure 3b) shows that the IPCE value of R-NRAs is higher than 60% in the wavelength range from 350 to 380 nm, indicating the charge carriers being effectively separated and transported in the R-NRAs. In the visible range, the IPCE values of R-NRAs are comparable to those of the NRAs. Hence, the enhancement of the photocurrent of R-NRAs is unlikely because of the extended light absorption induced by the disordered surface layer.

To further investigate the effect of the disordered layer on the electrical properties of R-NRAs, we conducted electrochemical impedance measurements. Figure 3c shows the Mott−Schottky plots of NRAs and R-NRAs obtained at a frequency of 1 kHz. It can be seen that the slope of R-NRAs is much smaller than that of the NRAs. The decreased slope implies the enhanced donor densities according to the Mott−Schottky equation[32]

$$N_d = (2/e_0\varepsilon\varepsilon_0)[d(1/C^2)/dV]^{-1}$$

Where N_d is the donor density, e_0 is the electron charge, ε is the dielectric constant of NRAs, ε_0 is the permittivity of vacuum, and V is the applied bias. The calculated carrier densities of the NRAs and R-NRAs are 4.9×10^{18} cm^{-3} and 1.6×10^{21} cm^{-3}, respectively. Apparently, electrochemical reduction leads to about 3 orders of magnitude enhancement in the carrier density of NRAs. The enhanced carrier density is likely due to the increased oxygen vacancies at the hydrogenated disordered shell,[25] which could facilitates the charge transport in NRAs as demonstrated in Figure 2. Moreover, the flat band position of R-NRAs shifts to −0.2 V vs RHE, suggesting a negative shift of the Fermi level, which might be attributed to the appearance of the shallow states in the disordered surface layer.

The performance of the surface hole injection was evaluated by Na_2SO_3 oxidation.[2,33] The charge separation efficiencies of the R-NRAs and NRAs electrodes were obtained by comparing the photocurrent from Na_2SO_3 oxidation with the theoretical maximum photocurrent (see Figure S12 in the Supporting Information). The charge separation curve of R-NRAs (Figure 4a) exhibits a higher fill factor than that of NRAs electrode. Another interesting feature is that the charge injection efficiency of R-NRAs (Figure 4b) is substantially increased to 100% at a potential of 1.23 V. The improved hole injection can be stemming from the shallow states energy levels in the surface disorder layer. As shown in Figure 4c, the shallow states energy levels can act as the intermediate lends for transferring the photogenerated holes from TiO_2 to semiconductor−electrolyte interface, leading to more efficient water oxidation.

To further support the above reasoning, we loaded the NRAs and R-NRAs with CoPi oxygen evolution catalyst. Figure 4b shows that the charge injection efficiency of bare NRAs electrode is very poor, indicating that photogenerated holes are initially accumulated on the surface. After introduction of CoPi, the charge injection efficiency of NRAs is substantially enhanced, reaching 74% at a potential of 1.23 V. In the meantime, the charge-injection efficiency curve of R-NRAs without CoPi loading is close to that of the CoPi/NRA electrode, confirming that the surface disordered layer promotes water oxidation as CoPi does. Figure 5 provides the electrochemical impedance spectroscopy (EIS) curves of

DOI: 10.1021/am508738d
ACS Appl. Mater. Interfaces 2015, 7, 3791−3796

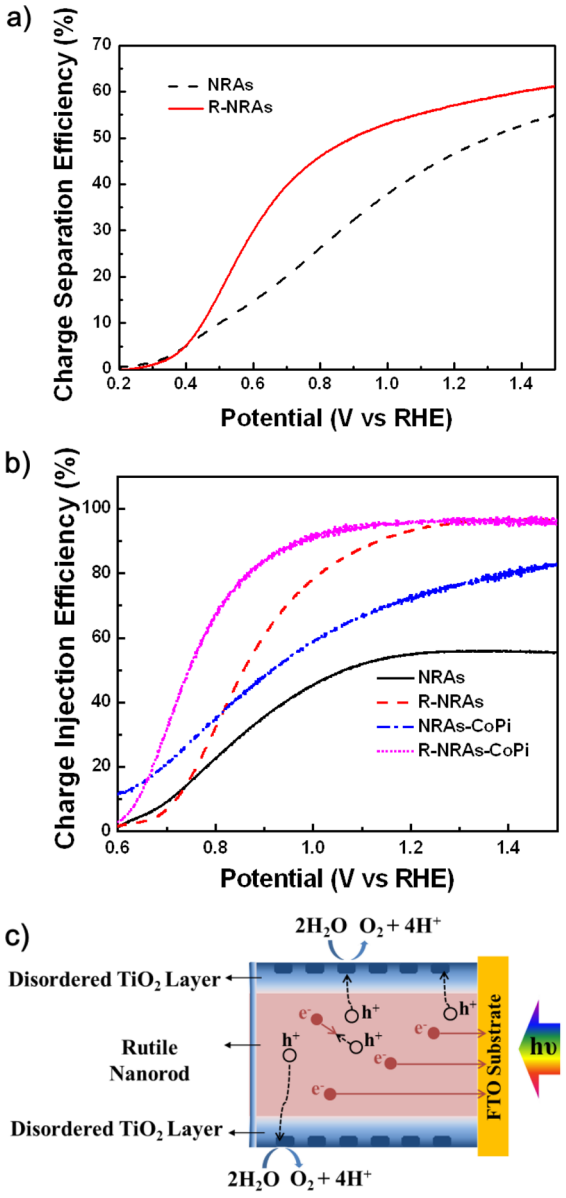

Figure 4. (a) Charge separation efficiency versus potential curves of the NRAs and R-NRAs photoanodes; (b) charge injection efficiency versus potential curves of the NRAs, CoPi/NRAs, R-NRAs and CoPi/R-NRAs; (c) cross-sectional schematic of the photoanode with a disorder shell for solar water splitting.

the above electrodes (the optimum fitting R and CPE values are provided in Table S1 in the Supporting Information). After the addition of CoPi, the diameter of the second arc (under the lower frequency) decreases significantly, while the diameter of the first arc (under the higher frequency) shows no obvious change. As already discussed elsewhere,[34] the first arc represents the charge-transfer step and the second arc corresponds to the surface water oxidation step. Both arcs of the R-NRAs significantly decrease revealing that the presence of surface disordered layer increases charge carrier transport inside the electrode and is beneficial for the surface water oxidation, which agrees well with the charge efficiency results as we previously mentioned. These results strongly prove that the charge transfer kinetics is largely facilitated by the surface disordered layer, which is similar to the function of CoPi.

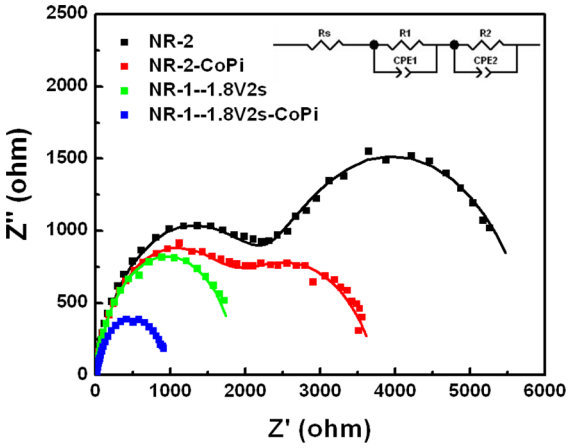

Figure 5. Electrochemical impedance spectra recorded as Nyquist plots in 0.5 M Na_2SO_4 at 0.64 V vs RHE. The experiment data is represented by discrete points and the simulated impedance response is represented by a solid line. The inset demonstrates the equivalent circuit used in the fitting of the impedance data.

4. CONCLUSION

We demonstrate that the R-NRAs electrode prepared with electrochemical reduction possesses disordered layer on the surface. The presence of such disordered TiO_2 surface layer on R-NRAs can substantially enhance the photocurrent of NRAs, up to 120% higher than that of the pristine NRAs electrode at 1.23 V vs RHE. Our characterizations indicate that the surface disordered layer facilitates the charge separation and collection at the semiconductor/electrolyte interface.

■ ASSOCIATED CONTENT

Supporting Information

Additional characterization data of the NRAs and R-NRAs, and a detailed table of derived R and CPE values of the EIS spectra are presented. This material is available free of charge via the Internet at http://pubs.acs.org.

■ AUTHOR INFORMATION

Corresponding Authors

*E-mail: ygan@hit.edu.cn. Tel: +86 45186413708.
*E-mail: canli@dicp.ac.cn. Tel: +86 41184379070.

Author Contributions

The manuscript was written through contributions of all authors. All authors have given approval to the final version of the manuscript.

Notes

The authors declare no competing financial interest.

■ ACKNOWLEDGMENTS

This work was financially supported by 973 National Basic Research Program of the Ministry of Science and Technology (2014CB239403), National Natural Science Foundation of China (21373209), the Fundamental Research Funds for the Central Universities (HIT. KISTP. 201406).

■ REFERENCES

(1) Hisatomi, T.; Kubota, J.; Domen, K. Recent Advances in Semiconductors for Photocatalytic and Photoelectrochemical Water Splitting. *Chem. Soc. Rev.* **2014**, *43*, 7520−7535.

DOI: 10.1021/am508738d
ACS Appl. Mater. Interfaces 2015, 7, 3791−3796

(2) Kim, T. W.; Choi, K. S. Nanoporous $BiVO_4$ Photoanodes with Dual-layer Oxygen Evolution Catalysts for Solar Water Splitting. *Science* **2014**, *343*, 990−994.
(3) Hong, S. J.; Lee, S.; Jang, J. S.; Lee, J. S. Heterojunction $BiVO_4$/WO_3 Electrodes for Enhanced Photoactivity of Water Oxidation. *Energy Environ. Sci.* **2011**, *4*, 1781−1787.
(4) Sang, L.; Zhao, Y.; Burda, C. TiO_2 Nanoparticles as Functional Building Blocks. *Chem. Rev.* **2014**, *114*, 9283−9318.
(5) Ding, C.; Shi, J.; Wang, D.; Wang, Z.; Wang, N.; Liu, G.; Xiong, F.; Li, C. Visible Light Driven Overall Water Splitting Using Cocatalyst/$BiVO_4$ Photoanode with Minimized Bias. *Phys. Chem. Chem. Phys.* **2013**, *15*, 4589−4595.
(6) Klahr, B.; Gimenez, S.; Fabregat-Santiago, F.; Bisquert, J.; Hamann, T. W. Electrochemical and Photoelectrochemical Investigation of Water Oxidation with Hematite Electrodes. *Energy Environ. Sci.* **2012**, *5*, 7626−7636.
(7) Li, Y.; Zhang, L.; Torres-Pardo, A.; Gonzalez-Calbet, J. M.; Ma, Y.; Oleynikov, P.; Terasaki, O.; Asahina, S.; Shima, M.; Cha, D.; Zhao, L.; Takanabe, K.; Kubota, J.; Domen, K. Cobalt Phosphate-modified Barium-doped Tantalum Nitride Nanorod Photoanode with 1.5% Solar Energy Conversion Efficiency. *Nat. Commun.* **2013**, *4*, 2566−2572.
(8) Wang, N.; Wang, D.; Li, M.; Shi, J.; Li, C. Photoelectrochemical Water Oxidation on Photoanodes Fabricated with Hexagonal Nanoflower and Nanoblock WO_3. *Nanoscale* **2014**, *6*, 2061−2066.
(9) Fujishima, A.; Honda, K. Electrochemical Photolysis of Water at a Semiconductor Electrode. *Nature* **1972**, *238*, 37−38.
(10) Liu, R.; Zheng, Z.; Spurgeon, J.; Yang, X. G. Enhanced Photoelectrochemical Water-splitting Performance of Semiconductors by Surface Passivation Layers. *Energy Environ. Sci.* **2014**, *7*, 2504−2517.
(11) Khan, S. U. M.; Al-Shahry, M.; Ingler, W. B. Efficient Photochemical Water Splitting by a Chemically Modified n-TiO_2. *Science* **2002**, *297*, 2243−2245.
(12) Liu, G.; Shi, J.; Zhang, F.; Chen, Z.; Han, J.; Ding, C.; Chen, S.; Wang, Z.; Han, H.; Li, C. A Tantalum Nitride Photoanode Modified with a Hole-Storage Layer for Highly Stable Solar Water Splitting. *Angew. Chem.* **2014**, *126*, 7423−7427.
(13) Shen, S.; Wang, X.; Ding, Q.; Jin, S.; Feng, Z.; Li, C. Effect of Pt Cocatalyst in Pt/TiO_2 Studied by in situ FTIR of CO Adsorption. *Chin. J. Catal.* **2014**, *35*, 1900−1906.
(14) Palomares, E.; Clifford, J. N.; Haque, S. A.; Lutz, T.; Durrant, J. R. Control of Charge Recombination Dynamics in Dye Sensitized Solar Cells by the Use of Conformally Deposited Metal Oxide Blocking Layers. *J. Am. Chem. Soc.* **2002**, *125*, 475−482.
(15) Hisatomi, T.; Le Formal, F.; Cornuz, M.; Brillet, J.; Tetreault, N.; Sivula, K.; Gratzel, M. Cathodic Shift in Onset Potential of Solar Oxygen Evolution on Hematite by 13-group Oxide Overlayers. *Energy Environ. Sci.* **2011**, *4*, 2512−2515.
(16) Hu, S.; Shaner, M. R.; Beardslee, J. A.; Lichterman, M.; Brunschwig, B. S.; Lewis, N. S. Amorphous TiO_2 Coatings Stabilize Si, GaAs, and GaP Photoanodes for Efficient Water Oxidation. *Science* **2014**, *344*, 1005−1009.
(17) Matsukawa, M.; Ishikawa, R.; Hisatomi, T.; Moriya, Y.; Shibata, N.; Kubota, J.; Ikuhara, Y.; Domen, K. Enhancing Photocatalytic Activity of LaTiO2N by Removal of Surface Reconstruction Layer. *Nano Lett.* **2014**, *14*, 1038−1041.
(18) Nurlaela, E.; Ould-Chikh, S.; Harb, M.; del Gobbo, S.; Aouine, M.; Puzenat, E.; Sautet, P.; Domen, K.; Basset, J.-M.; Takanabe, K. Critical Role of the Semiconductor−Electrolyte Interface in Photocatalytic Performance for Water-Splitting Reactions Using Ta_3N_5 Particles. *Chem. Mater.* **2014**, *26*, 4812−4825.
(19) Hwang, Y. J.; Hahn, C.; Liu, B.; Yang, P. Photoelectrochemical Properties of TiO_2 Nanowire Arrays: A Study of the Dependence on Length and Atomic Layer Deposition Coating. *ACS Nano* **2012**, *6*, 5060−5069.
(20) Chen, X.; Liu, L.; Liu, Z.; Marcus, M. A.; Wang, W. C.; Oyler, N. A.; Grass, M. E.; Mao, B.; Glans, P. A.; Yu, P. Y.; Guo, J.; Mao, S. S. Properties of Disorder-Engineered Black Titanium Dioxide Nanoparticles through Hydrogenation. *Sci. Rep.* **2013**, *3*, 1510−1516.
(21) Liu, N.; Schneider, C.; Freitag, D.; Venkatesan, U.; Marthala, V. R. R.; Hartmann, M.; Winter, B.; Spiecker, E.; Osvet, A.; Zolnhofer, E. M.; Meyer, K.; Nakajima, T.; Zhou, X.; Schmuki, P. Hydrogenated Anatase: Strong Photocatalytic Dihydrogen Evolution without the Use of a Co-Catalyst. *Angew. Chem.* **2014**, *53*, 14201−14205.
(22) Tan, H.; Zhao, Z.; Niu, M.; Mao, C.; Cao, D.; Cheng, D.; Feng, P.; Sun, Z. A Facile and Versatile Method for Preparation of Colored TiO2 with Enhanced Solar-driven Photocatalytic Activity. *Nanoscale* **2014**, *6*, 10216−10223.
(23) Xia, T.; Zhang, W.; Li, W.; Oyler, N. A.; Liu, G.; Chen, X. Hydrogenated Surface Disorder Enhances Lithium Ion Battery Performance. *Nano Energy* **2013**, *2*, 826−835.
(24) Chen, X.; Liu, L.; Yu, P. Y.; Mao, S. S. Increasing Solar Absorption for Photocatalysis with Black Hydrogenated Titanium Dioxide Nanocrystals. *Science* **2011**, *331*, 746−750.
(25) Wang, G.; Wang, H.; Ling, Y.; Tang, Y.; Yang, X.; Fitzmorris, R. C.; Wang, C.; Zhang, J. Z.; Li, Y. Hydrogen-Treated TiO_2 Nanowire Arrays for Photoelectrochemical Water Splitting. *Nano Lett.* **2011**, *11*, 3026−3033.
(26) Zhou, H.; Zhang, Y. Electrochemically Self-Doped TiO2 Nanotube Arrays for Supercapacitors. *J. Phys. Chem. C* **2014**, *118*, 5626−5636.
(27) Xie, S.; Zhai, T.; Li, W.; Yu, M.; Liang, C.; Gan, J.; Lu, X.; Tong, Y. Hydrogen Production from Solar Driven Glucose Oxidation over $Ni(OH)_2$ Functionalized Electroreduced-TiO2 Nanowire Arrays. *Green Chem.* **2013**, *15*, 2434−2440.
(28) Liu, B.; Aydil, E. S. Growth of Oriented Single-Crystalline Rutile TiO2 Nanorods on Transparent Conducting Substrates for Dye-Sensitized Solar Cells. *J. Am. Chem. Soc.* **2009**, *131*, 3985−3990.
(29) Di Valentin, C.; Pacchioni, G.; Selloni, A. Reduced and n-Type Doped TiO2: Nature of Ti3+ Species. *J. Phys. Chem. C* **2009**, *113*, 20543−20552.
(30) Macdonald, I. R.; Rhydderch, S.; Holt, E.; Grant, N.; Storey, J. M. D.; Howe, R. F. EPR Studies of Electron and Hole Trapping in Titania Photocatalysts. *Catal. Today* **2012**, *182*, 39−45.
(31) Kumar, C. P.; Gopal, N. O.; Wang, T. C.; Wong, M. S.; Ke, S. C. EPR Investigation of TiO_2 Nanoparticles with Temperature-dependent Properties. *J. Phys. Chem. B* **2006**, *110*, 5223−5229.
(32) Rajeshwar, K. Fundamentals of Semiconductor Electrochemistry and Photoelectrochemistry. In *Encyclopedia of Electrochemistry*; Wiley−VCH: Weinheim, Germany, 2002.
(33) Seabold, J. A.; Choi, K. S. Efficient and Stable Photo-oxidation of Water by a Bismuth Vanadate Photoanode Coupled with an Iron Oxyhydroxide Oxygen Evolution Catalyst. *J. Am. Chem. Soc.* **2012**, *134*, 2186−2192.
(34) Liu, H.; Li, X. Z.; Leng, Y. J.; Li, W. Z. An Alternative Approach to Ascertain the Rate-Determining Steps of TiO_2 Photoelectrocatalytic Reaction by Electrochemical Impedance Spectroscopy. *J. Phys. Chem. B* **2003**, *107*, 8988−8996.

DOI: 10.1021/am508738d
ACS Appl. Mater. Interfaces 2015, 7, 3791−3796